

P14R.10 Radar, Lidar, and In-situ Observations of Tropical Cirrus Clouds

L. R. Belcher¹ and G. M. Heymsfield²

¹ Science Systems and Applications Inc., Lanham, MD

² NASA/Goddard Space Flight Center, Greenbelt, MD

1. Introduction

The global distribution, microphysical, and dynamical properties of cirrus clouds have prompted many studies aimed at a better understanding of their impact on the Earth's radiation budget (Stephens et al. 1981, 1990; Liou 1986; Sassen 2002; Stephens 2002). Much of this effort is directed at improving simulations of the lifecycle, from formation to decay, of these important ice-phase clouds in weather and climate models (Starr and Cox, 1985; Jensen and Pfister, 2004; Jensen et al., 2005). Interest in tropopause cirrus layers includes investigations into their role in upper tropospheric dehydration (e.g., Jensen and Pfister, 2004), the influence of the indirect aerosol effect on their formation (Sassen et al., 2003), and the connection between lower troposphere convection and cirrus clouds (Garrett et al., 2004; Massie et al., 2002). While the horizontal (and vertical to some extent) distribution of cirrus clouds is readily obtained from satellite observations, a detailed understanding of the complex microphysical and dynamical processes within cirrus layers remains a challenge. This study examines several unique features of tropical cirrus clouds utilizing data from remote-sensing and in-situ platforms that were deployed during the NASA CRYSTAL-FACE (CF henceforth) field program in July 2002.

2. Convective intensity and cirrus coverage during CRYSTAL-FACE

Cloud features that were present during the CF field program provide insight into the synoptic conditions and weather events within the region of interest. By using geo-stationary satellite data (GOES-8), we investigate convective intensity and total anvil coverage over south Florida. The analysis of the infrared (10.6 μ m) GOES-8 data for this study includes a $4^\circ \times 4^\circ$ region centered at the CF western ground site (25 deg 53.0 min N, 81 deg 19.0 min W). We processed each of the GOES-8 images (~30 min scans) from each day to produce plots of minimum infrared brightness temperature (T_b) (Figure 1, upper panel) and areal coverage at selected T_b thresholds ranging from 212 to 230 $^\circ$ K (Fig. 1, lower panel).

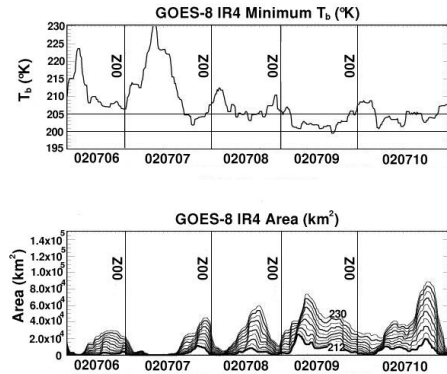


Figure 1. GOES-8 IR4 T_b minimum and areal coverage from 6 – 10 July, 2002.

The trend of minimum T_b is an excellent indicator of convective intensity (within the region of GOES-8 data used in this study) since low T_b observations are typically associated with intense thunderstorms and strong updrafts (Adler and Mack, 1986; Heymsfield et al., 1991). Intense convection was abundant (within the selected region) on 9 and 10 July as seen by the extended periods in which the IR T_b remained below 205 $^\circ$ K. Deep convection also occurred on 18, 19, 21, and 26 July (not shown here) with minimum T_b observations falling below 200 $^\circ$ K. The 8, 9, and 10 July days shown in Fig. 1 exhibit some of the most widespread anvil coverage during CF, based on areal coverage of the warmest (230 $^\circ$ K) IR threshold. The diurnal variation of the convection is also obvious from Fig. 1.

3. Radar and lidar Intercomparison

High-resolution radar and lidar observations reveal the complex, multi-layered cloud structure in many of the storms observed. By combining observations from the NASA Cloud Radar System (CRS; Li et al., 2004) and Cloud Physics Lidar (CPL; McGill et al., 2002), we investigate differences between radar- and lidar-observed cloud top and relate these differences to other observables (e.g., lidar-derived cloud optical depth). The CPL is sensitive to small cloud particles and is able to detect optically thin cirrus layers that CRS is typically unable to resolve. However, in many cases the lidar signal is completely attenuated in the upper regions of the

cloud while CRS is able to penetrate further into the cloud. McGill et al. (2004) provide a comprehensive statistical intercomparison between these two instruments and demonstrate how measurements from each of these instruments compliment each other, thus highlighting their potential benefits to future cloud observation platforms (e.g., validation of the NASA A-train; Stephens et al., 2002).

One interesting CF case with convection embedded within cirrus cloud is shown in Figure 2. The CPL attenuated backscatter image (not shown) indicated a multi-layered cirrus cloud with a thin tenuous layer residing above a more robust cirrus layer. The cloud top height estimate from CPL clearly shows this layer, while the CRS cloud top estimate indicates the height of the more developed cirrus layer. The two instruments come into agreement (w.r.t., cloud top estimate) over a convective tower (~140 km along the flight track). During the NASA ER-2 overpass, the NASA WB-57 flew a coincident pass within the cloud layer (highlighted in Fig. 2), providing in-situ particle measurement of this cloud. The particle size distribution (PSD) from the merged SPP, CAPS, and CPI instruments indicated a wider PSD with larger particles during the lower pass (not shown) in the region of cloud detected by CRS. However, during the return pass at a higher altitude, the PSD was not as wide and the largest particles observed were below 300 m. It is in this region that the CPL detected cloud, while the CRS did not resolve this tenuous layer.

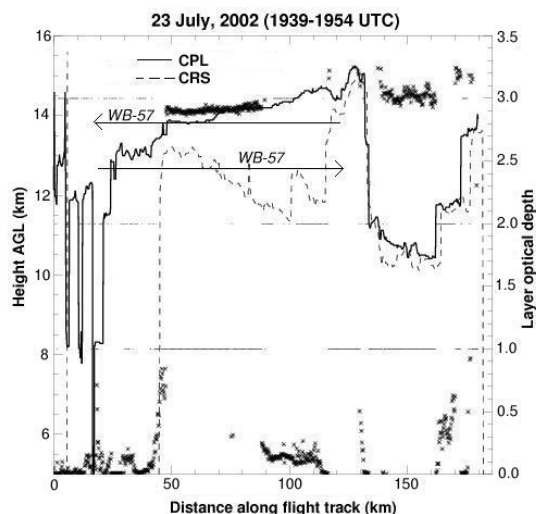


Figure 2. Comparison of CPL (solid) and CRS (dashed) cloud top along ER-2 flight track on 23 July, 2002. Layer optical depth and number of layers observed from CPL are also shown (asterisk and thin line respectively).

4. Cirrus complexity and environmental conditions

Thin tropopause cirrus layers (TTC) were

ubiquitous during many of the missions (e.g., 23 July case shown above), yet they were seldom observed during the final flight of the field campaign (see Table 1). Highlighted in Table 1 is the 7 July case, in which the clouds sampled on this day exhibited complex, multi-layered structure. Also highlighted is the 29 July case, which shows the majority of the CPL profiles indicated a single cirrus layer. The change in complexity of the cirrus layers during these two cases warrant further investigation into the environmental conditions that might have brought about these differences.

During most of the CF experiment, a ridge of high pressure resided over central Florida with light winds in the upper levels. However, NCEP/NCAR model re-analysis data shows that near the end of July, an approaching easterly wave modified the synoptic conditions in the region. This wave and associated changes in the environment likely contributed to the scarcity of the TTC layers on the final day of the mission. The time history of sounding data from Miami and Tampa (not shown) indicated stronger vertical wind shear and upper level winds during the latter days of the CF mission. Additionally, the sounding analysis indicated lower relative humidity (w.r.t. ice) observations at 200 mb in the 28-29 July time frame. These combined effects (i.e., stronger wind shear and lower RH) likely played a key role in cirrus formation and lack of complexity in the TTC observed on the final CF mission.

Date	1 Layer	2 Layers	3 Layers
3 July	3072	603	48
7 July	8478	4594	476
9 July	7148	1758	296
13 July	7544	643	72
19 July	4903	1740	104
23 July	3759	1482	207
26 July	4185	743	53
28 July	5624	1385	247
29 July	6719	438	3

Table 1. Number of one second CPL profiles that a given number of cirrus layers were observed above 10 km (AGL).

5. Discussion and Future Work

We have utilized radar and lidar observations of tropical convection and the associated formation of cirrus anvils from CF in order to demonstrate the complimentary nature of these two instruments for this type of study. We have investigated differences between radar- and lidar-observed cloud top and cirrus structure as

they relate to the regional environmental conditions (e.g., temperature, humidity, and winds). In several cases, properties of the TTC layers were sampled in-situ, providing information on ice particle size distributions, which helped explain differences (e.g., sensitivity) in the CRS and CPL observations.

The primary goal of this work is to gain an enhanced understanding of the connections between the synoptic environment and the formation of cirrus and TTC layers associated with tropical convection. We have thus far utilized a limited set of observations and hope to add additional case studies in order to further understand these connections. In addition to further analysis of cirrus lifecycle and complexity, we seek to better understand the role of convection and mass detrainment in the formation of cirrus layers in future work.

Acknowledgments

This effort was supported by NASA's Radiation Sciences Program at NASA HQ. We thank Drs. Lihua Li and Lin Tian for their careful efforts on CRS instrumentation, data set, and analysis. We would also like to thank Dr. Matthew McGill and Mr. Dennis Hlavka for providing the CPL data used here. We also appreciate the efforts of the NOAA-CIRES Climate Diagnostics Center in the production of the NCEP/NCAR model re-analysis data.

References

Adler, R. F., and R. A. Mack, 1986: Thunderstorm cloud top dynamics inferred from satellite observations and a cloud top parcel model. *J. Atmos. Sci.*, **43**, 1945-1960.

Heymsfield, G. M., R. Fulton, and J. D. Spinhirne, 1990: Aircraft overflight measurements of midwest severe storms: Implications on geosynchronous satellite interpretations. *Mon. Wea. Rev.*, **119**, 436-456.

Jensen, E., L. Pfister, T. Bui, A. Weinheimer, E. Weinstock, J. Smith, J. Pittman, D. Baumgardner, P. Lawson, and M. J. McGill, 2005: Formation of a tropopause cirrus layer observed over Florida during CRYSTAL-FACE. *J. Geophys. Res.*, **110**, D03208, doi:10.1029/2004JD004671.

- , and L. Pfister (2004), Transport and freeze-drying in the tropical tropopause layer. *J. Geophys. Res.*, **109**, D02207, doi:10.1029/2003JD004022.

Li, L., G. M. Heymsfield, P. E. Racette, L. Tian, and E. Zenker, 2004: A 94 GHz cloud radar system on a NASA high-altitude ER-2 aircraft. *J. Atmos. Oceanic Technol.*, **21**, 1378-1388.

Liou, K.-N., 1986: Influence of cirrus clouds on weather and climate processes: A global perspective. *Mon. Wea. Rev.*, **114**, 1167-1199.

Massie, S., A. Gettelman, W. Randel, and D. Baumgardner, 2002: Distribution of tropical cirrus in relation to convection. *J. Geophys. Res.*, **107**, 4591, doi:10.1029/2001JD001293.

McGill, M. J., D. L. Hlavka, W. D. Hart, V. S. Scott, J. D. Spinhirne, and B. Schmid, 2002: The cloud physics lidar: Instrument description and initial measurement results. *Appl. Opt.*, **41**, 3725-3734.

- , L. Li, W. D. Hart, G. M. Heymsfield, D. L. Hlavka, P. E. Racette, L. Tian, M. A. Vaughan, and D. M. Winker, 2004: Combined lidar-radar remote sensing: Initial results from CRYSTAL-FACE. *J. Geophys. Res.*, **109**, D07203, doi:10.1029/2003JD004030.

Starr, D. O'C., S. K. Cox, 1985: Cirrus Clouds. Part I: A Cirrus Cloud Model. *J. Atmos. Sci.* **42**, 2663-2681

Stephens, G. L., 2002: Cirrus, climate, and global change. *Cirrus*, D. K. Lynch et al., Eds., Oxford University Press, 433-448.

- , et al., 2002: The Cloudsat mission and the A-Train: A new dimension of space-based observations. *Bull. Amer. Meteor. Soc.*, **83**, 1771-1790.

- , S.-C. Tsay, J. P. W. Stackhouse, and P. J. Flatau, 1990: The relevance of the microphysical and radiative properties of cirrus clouds to climate and climatic feedback. *J. Atmos. Sci.*, **47**, 1742-1753.

- , G. G. Campbell, and T. H. Vonder Haar, 1981: Earth radiation budgets. *J. Geophys. Res.*, **86**, 9739-9760.